Nanoscale

Accepted Manuscript

This article can be cited before page numbers have been issued, to do this please use: S. Pothorszky, D. Zámbó, T. Deák and A. Deák, *Nanoscale*, 2016, DOI: 10.1039/C5NR08014B.

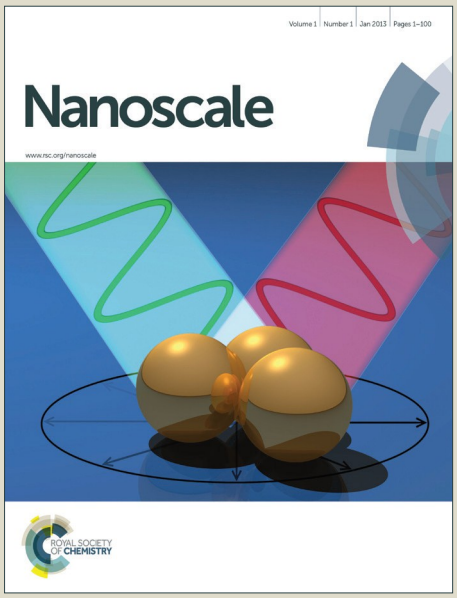

ROYAL SOCIETY OF CHEMISTRY

www.rsc.org/nanoscale

View Article Online
DOI: 10.1039/C5NR08014B

Nanoscale

ARTICLE

Assembling patchy nanorods with spheres: Limitations imposed by colloidal interactions

Received 00th January 20xx,
Accepted 00th January 20xx

DOI: 10.1039/x0xx00000x

www.rsc.org/Nanoscale

Sz. Pothorszky,[a] D. Zámbó, [a] T. Deák, [b] A. Deák. [a]

For gold nanorods the intrinsic shape-anisotropy offers the prospect of anisotropic assembly, provided their region-selective surface modification can be realized. Here we developed a nanorod with patchy surface chemistry, featuring positively charged molecules in the tip region and polymer molecules at the sides by careful control of molecule concentrations during ligand exchange. When these patchy nanorods are assembled with small negatively spherical particles, electric double layer interaction can direct the assembly of two nanospheres at the opposite ends of the nanorods. The PEG chains promote the selectivity of the procedure. As the size of the nanospheres increases, they start to shift towards the side of the nanorod due to increased van der Waals interaction. When the relative size of the nanospheres is even larger, only a single nanoshpere is assembled, but instead of the tip region, they are attached to side of the nanorods. The apparent cross-over of the region-selectivity can be interpreted in terms of colloidal interactions, i.e. the second spherical particle is excluded due to nanosphere-nanosphere electric double layer repulsion, while the large vdW attraction result in a side positioning of the single adsorbed spherical particle. The results underline the importance of absolute values of the different interaction strengths and length scales in the programmed assembly of pathy nanoscale building blocks.

Introduction

In the absence of external fields, the directed assembly of nanoparticles can be realized based on colloidal[1] or other bio-specific interactions.[2,3] Mastering the positioning in nanoparticle assemblies is a great challenge but a number of applications could benefit from it, like catalysis,[4] biomedical applications,[5] surface-enhanced Raman scattering (SERS)[6] or nanoparticle networks.[7,8] The majority of chemically triggered nanoscale assembly procedures rely on the intrinsic surface properties of the building blocks.[9] The size and shape of the particles has also significant influence on the resulting structure. Rod-like objects can benefit simultaneously from shape and surface chemistry anisotropy (patchiness), making them excellent candidates for directed assembly.[10,11] Three- and two-dimensional self-assembled superstructures composed simultaneously of gold nanorods (AuNRs) and nanospheres (AuNPs) have been prepared earlier by different methods, e.g. by depletion interaction at high particle densities,[12] but in most cases the assembly from dilute systems is carried out by making use of the selective surface modification of the anisometric nanorods. One of the most successful approaches for complex assemblies is based on the specific interaction between complementary DNA strands.[2] Generally, colloidal interactions can also be used to direct the assembly of nanorods and nanoparticles,[13-15] but since they are less specific compared to the DNA based approaches, strategies involving region-selective surface modification leading to a patchy surface chemistry can provide a better control over the resulting structure.[16,17] Cetyltrimethylammonium bromide (CTAB) stabilised gold nanorods offer the possibility for region-selective surface modification due to the less compact ligand shell at the tip region. By careful controlling the concentration of thiol-containing molecules during ligand exchange, selective tip-functionalization of the rods can be achieved,[18-20] whereas higher concentrations result in the complete replacement of the CTAB molecules by the thiols. Treating the tip region of the NRs with charged thiol molecules can enable the preparation tip-assembled superstructures via electrostatic interactions.[21]

In this work the self-assembly of region-selectively surface modified patchy gold nanorods and spherical gold nanoparticles is investigated. A robust two-step surface modification procedure was applied to prepare patchy gold nanorods with spatially inhomogeneous surface-ligands. First the tip of the rods was functionalized with positively charged cysteamine, then the CTAB molecules at the side of the rods

[a] Institute for Technical Physics and Materials Science, HAS Centre for Energy Research, P.O. Box 49, H-1525 Budapest, Hungary
[b] Institute of Viticulture and Oenology, Corvinus University of Budapest, H-1118 Budapest, Villányi út 29-43.
† Footnotes relating to the title and/or authors should appear here.
Electronic Supplementary Information (ESI) available: See DOI: 10.1039/x0xx00000x

View Article Online
DOI: 10.1039/C5NR08014B

were replaced by thiol-functionalized methoxy-polyethylene glycol (mPEG-SH). These patchy particles were self-assembled with negatively charged, citrate stabilized spherical particles of different sizes. The assembly process was followed by ensemble optical extinction measurements and the results were interpreted based on optical simulations and scanning electron microscopy. We show that the mPEG-SH coating on the side of the rods can effectively promote the tip-selective binding of two nanospheres at the opposite ends of the rod. As the relative size of the spherical particles increases, however, the two particles are shifted around the perimeter of the nanorod, and finally only a single sphere gets assembled at the side of the rods. The findings can be interpreted in terms of colloidal interactions and highlight the importance of the length scales regarding surface inhomogeneity vs. object sizes. It also draws attention to the limitations of colloidal interaction base directed assembly of patchy nanoparticles.

Experimental

Gold nanoparticle synthesis and surface modification

Sodium citrate tribasic dihydrate (ACS reagent, ≥99.0%), cetyltrimethylammonium bromide (CTAB, 99%), sodium borohydride (NaBH4, 99%), L-ascorbic acid (AA, >99%), silver nitrate (AgNO3, >99%), cysteamine hydrochloride (>99%), (11-Mercaptoundecyl)trimethylammonium bromide (TMA, >99%), hydrochloric acid (37%) and tetrachloroauric acid trihydrate (99.9%) were obtained from Sigma-Aldrich. Thiol-functionalized methoxy-polyethylene glycol (mPEG-SH; MW=5000 Da) was supplied by RappPolymere GmbH. All chemicals were used as received. For all experiments, ultrapure water with a resistivity of 18.2 MΩ·cm was used.
Spherical gold nanoparticles with a diameter of 19 nm were prepared using the traditional Turkevich method.[22] These particles were also used for the preparation of larger, 40 nm diameter particles by using modified seeded three-step growth method.[23] The nanorod samples (54x15 nm; 60x16 nm; 80x21 nm) were prepared according to previously published seed-mediated protocol.[24]

Patchy nanorod preparation

For the preparation of patchy nanorods 10 ml 0.4 nM AuNR solution was centrifuged at 6000 rcf for 30 min and 90% of the supernatant was removed and the particles redispersed in Milli-Q water to set the CTAB concentration to 10 mM. 25 mM 0.1 ml cysteamine hydrochlorid was added dropwise to the nanorods and stirred gently for 30 min. Then 0.1 ml 10 mM (0.0125 g in 0.25 ml water) mPEG-SH (5 kDa) was added to 9.9 ml of cysteamine treated AuNR solution and stirred gently for 2 h. The resulting patchy AuNRs were purified by centrifuging two times at 6000 rcf for 30 min. For the preparation of only mPEG or only TMA covered AuNRs, the as-prepared nanorod solution was centrifuged and 0.1 ml 40 mM mPEG-SH or 0.1 ml 200 mM aqueous TMA solution were added to 9.9 ml AuNR solution. The solutions were stirred gently for 2 hours, then purified by centrifuging at 6000 rcf for 30 min. Preparation of only mPEG and TMA covered AuNRs were necessary for the almost complete removal CTAB from the system to serve as reference samples for steric or electric double layer dominated interaction during the assembly experiments.

Self-assembly procedure

For the spectral measurements, first the pH of the patchy particle's solution was adjusted to 6 using 1 mM HCl. Second, the as-prepared citrate stabilized AuNPs were 1:3 diluted with 1 mM citrate solution to set the concentration of nanospheres to 1.5 nM and the two solutions were mixed to result a nanosphere:nanorod molar ratio of 10:1. For SEM analysis the Si substrates (5x5 mm) were rinsed with acetone, isopropanol and finally with water and dried in nitrogen flow. The sample preparation for the SEM was implemented by spin-coating. Just before spin-coating, the substrates were plasma cleaned for 5 min, then 0.2 ml of 0.15 nM patchy AuNR solution (pH~6) was spin-coated at 2800 rpm for 30 s. 0.2 ml 1.5 nM nanosphere solution was drop-casted onto the substrate and left undisturbed for 1 min, after which the fluid was removed by pipette and the remaining droplets were blown off by a gentle nitrogen stream.

Characterization techniques

The synthesis and self-assembly of gold nanoparticles were monitored using a fibre coupled UV–Vis spectrometer (Thorlabs CCS200). Electrophoretic mobility measurements were carried out using dynamic light scattering (Malvern Zetasizer NanoZS). Scanning electron microscope (SEM) images were obtained using a Zeiss LEO field emission scanning electron microscope operated at 5 keV acceleration voltage. The interaction potential between spherical particles and the van der Waals attraction between a nanosphere and a nanorod was calculated as reported earlier.[25,13] Optical simulations were carried by boundary element method (BEM) out based on an open source Matlab® package developed by Hohenester and Trügler.[26] For the simulations, the rod and sphere dimensions were obtained from the experiments and the embedding medium was set to water.

Results and discussion

For the self-assembly experiments different nanoparticles with different surface modification were used. The central building block consisted of a nanorod with a patchy surface modification, i.e. a positively charged tip-region and a side-region covered by neutral mPEG-SH chains. The 'probe' particles for the assembly with the rods were citrate stabilized spherical gold particles with the sizes of 19 and 40 nm. To support our results on the region-selective surface modification of the rods and to underpin the robustness of the patchy particle in the self-assembly process, rods covered only by mPEG-SH or TMA were also prepared.

View Article Online
DOI: 10.1039/C5NR08014B

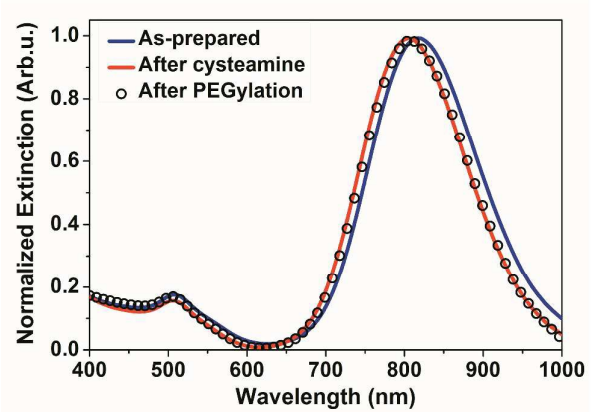

Figure 1. Extinction spectra of the as-prepared (blue) and cysteamine functionalized (red) gold nanorods (60x16 nm). There is no significant change in the extinction spectra after PEGylation (black empty dots).

While the assembly performed with the purely mPEG-SH covered particles gives information about the effectiveness of steric protection against sphere attachment, the complete TMA coating renders the rods permanently and highly positively charged and can be used to verify the electric double layer dominated nature of the assembly process. Extinction spectra of these simpler particle types, i.e. particles with a single surface chemistry flavour (mPEG-SH or TMA only), as well as the starting particles can be found in the Supporting Information (Figure S1-2).

Patchy gold nanorods

First, Au NRs with tip-selectively surface modification were prepared using cysteamine-hydrochloride, starting from CTAB capped NRs. Cysteamine-hydrochloride gives pH-dependent positive surface charge to the AuNRs, which allows tuning of the electric double layer interaction potential during rod-sphere assembly. The amount of the cysteamine molecules was optimized to bind mainly to the tip of the AuNRs. The second step of the procedure was the replacement of CTAB at the side region with mPEG-SH. It was imperative to fine-tune the mPEG-SH concentration, because the bound cysteamine molecules can be removed from the nanorod tip at high mPEG-SH concentrations. To assess the effectiveness and selectivity of the surface modification steps, extinction and electrokinetic measurements have been carried out. The characteristic extinction spectra at the three stages of the process are shown in Figure 1. Generally, cysteamine addition resulted in a significant blueshift of the original longitudinal resonance peak. This can be attributed to the increasing water volume fraction in the near-field region at the tips as a result of CTAB displacement by the short cysteamine molecules. On the contrary, no significant redshift of the longitudinal surface plasmon resonance (LSPR) peak was detectable after PEGylation, indicating that mPEG-SH leaves the already cysteamine covered tip-region intact, since for fully PEGylated nanorods the LSPR is identical to as-prepared particles (also see Supporting Information, Figure S2).

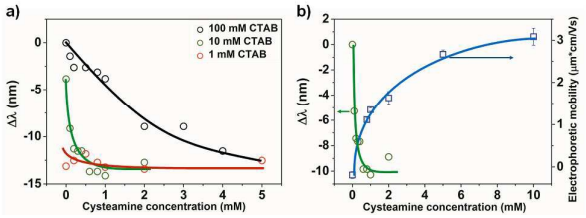

Figure 2. (a) Plot of the LSPR wavelength as a function of cysteamine concentration, for three different bulk CTAB concentrations. (b) Plot of the longitudinal peak position (left axis) and the measured with electrophoretic mobility values (right axis) of patchy particles as a function of cysteamine concentration. The solid lines in each graph are guidelines.

The measured spectral shift depends heavily on the cysteamine concentration. In Figure 2.a the longitudinal peak position as a function of cysteamine concentrations is shown. The value of the blueshift correlates with the added cysteamine amount. It has to be noted, that the observed blueshift also depends on the initial bulk concentration of CTAB. When setting lower CTAB concentrations than 100 mM (as-synthetized), one obtains a smaller longitudinal resonance wavelength value already for the starting sample, indicating the loosening and partial removal of the bilayer from the tips.[27]

While this partial removal certainly facilitates the thiol binding, at 1 ca. mM bulk CTAB concentration no modulation of the LSPR with the cysteamine concentration was detectable. Consequently the CTAB concentration was set to 10 mM for the preparation of patchy nanorods, because in this case the CTAB layer at the rod tip is already weakened but still compact at the side of the rods, providing the necessary region-selective cysteamine adsorption. [19]

After PEGylating the rods with 0.1mM mPEG-SH, the samples were found to be as stable as the fully PEGylated rods, while leaving the tip-region of the particles unaffected, i.e. no redshift of the LSPR peak was detectable upon PEGylation. While the LSPR shift provides information mainly about the refractive-index change at the rod tip, the electro-kinetic data characterizes the whole rod surface. In Figure 2.b the results of electrophoretic mobility measurements of the patchy particles are shown together with corresponding LSPR peak position as a function of cysteamine concentration used in the first surface modification step. The fully PEGylated nanorods (zero cysteamine concentration) have an electrophoretic mobility around zero. As the concentration of cysteamine increases, the electrophoretic mobility gradually increases as well, reaching +3 µmcm/Vs at 10 mM cysteamine concentration. It is important to point out, that the LSPR peak position reaches its final value already around 1 mM cysteamine concentration, but the electrophoretic mobility increases up to 10 mM. Based on these results, at 10 mM CTAB concentration selective surface modification of the tips is only possible below ca. 1 mM cysteamine concentration, above which no further attachment takes place at the tips, while adsorption at the rod as a whole certainly proceeds up to the 10 mM. Accordingly, 0.25 mM was chosen for the patchy particle preparation, at

View Article Online
DOI: 10.1039/C5NR08014B

which the almost maximum LSPR shift is accompanied by a marginal electrophoretic mobility change.

Assembly using nanorods with homogeneous surface chemistry

First of all as reference experiments two extreme conditions of the assembly were investigated, assembling fully TMA coated or fully PEGylated gold nanorods with 19 nm citrate stabilized spherical nanoparticles (zeta-potential: -31 mV). For both rod types, region-selective assembly cannot be expected, but they show the effectiveness of the electric double layer attraction and the steric repulsion, concerning the rod-sphere interaction. With the homogeneously TMA coated particles one can see how an assembled structure would look like with no region-selective surface distribution of the positively charged molecules, while for the fully PEGylated sample the effectiveness of steric blocking can be verified. The results are summarized in Figure 3. For the fully TMA coated particles, the SEM image in Figure 3.a indicates the high tendency of the oppositely charged spherical particles to assemble with the rods; multiple particles are gathered around a single rod in the form of small aggregates. The complete lack of site-selective assembly is also evident from the image. The observed structure can be interpreted in terms of the characteristics of the TMA coating: the thiol containing molecule covers the rod surface homogeneously due to the large excess during the ligand exchange as well as its high affinity to the gold surface and it has a permanent positive charge, resulting in +4 μmcm/Vs electrophoretic mobility.[28] As a consequence a large number of negatively charged particles adsorbed evenly around the rods. The observed structure correlates well with bulk-assembly experiments followed by extinction measurements. Upon bringing the TMA coated rods together with the negatively charged spheres in solution, significant redshift and broadening both in the transversal and longitudinal plasmon modes can be observed (Figure 3.c). This originates from the coupled modes arising due to homogenous adsorption of the spherical particles at the nanorods and also most probably due to the formation chain and fractal like aggregates.

On the other hand, when assembling the spherical nanoparticles with the fully PEGylated rods, no attachment of the spheres to the rods can be observed. Instead, there is a clearly depleted empty zone around the rods (Figure 3.b). This can be attributed to the effective steric repulsion of the PEG chains that prevents close approach of the spherical particles, just like observed earlier for a sphere-only system.[25] The depth of this zone is around 15±1 nm and correlates well with the 17 nm thickness of a PEG (MW= 5 kDa) layer grafted on a gold surface.[29] This reluctance of the nanospheres to attach to the rods is well reflected in the ensemble spectra measured during the assembly in the bulk: no change in the longitudinal or transversal peaks could be observed, but the presence of the spherical particles in the mixed solution is clear from their dipole resonance peak around 530 nm (Figure 3.d).

Assembly using patchy nanorods

The patchy particles were assembled with spherical negatively charged particles in the same way as the rods with homogeneous surface chemistry. In Figure 4.a characteristic SEM image of the assembled structure based on patchy nanorods and 19 nm spheres is shown. First, it is obvious, that the rods preferentially (ca. 70%) accumulate two spheres in their tip regions at the opposite ends of the rod. Second, it is also clear, that instead of a perfect end-positioning, the spheres are usually side-shifted compared to the long axis of the rod. Previously it was argued, that generally the tip-attachment of the spheres can be attributed to the induced dipole interaction between the rod and the sphere.[13] It is important to point out, however, that our system is markedly different due to the spatially inhomogeneous surface modification of the rods. Based on the control experiment performed with the only TMA or PEG coated rods (Figure 3.) it is the region-selective surface-modification, that enables the attachment of the spherical particles to the rod tips, due to the electric double layer attraction between the oppositely charged rod tip and the spheres. The observed lateral displacement of the spheres might be attributed to the difference in the van der Waals attraction for the side and tip locations.[14] This difference is ca. 50% for the present system in favour of the side arrangement (see Supporting Information for details), which is apparently effectively counterbalanced by the steric repulsion exerted on the spheres by the PEG chains, not allowing a complete downshift along the rod perimeter. The ensemble extinction spectra measured in solution upon assembly (Figure 4.b) show a clear redshift of the longitudinal band position, but the position of transversal mode is not affected by the spherical particles. This finding, together with the simulation of the transversal (Figure 4.c) and longitudinal mode (Figure 4.d) suggests that the tip-located spheres are moving to the side position only after drying of the sample.

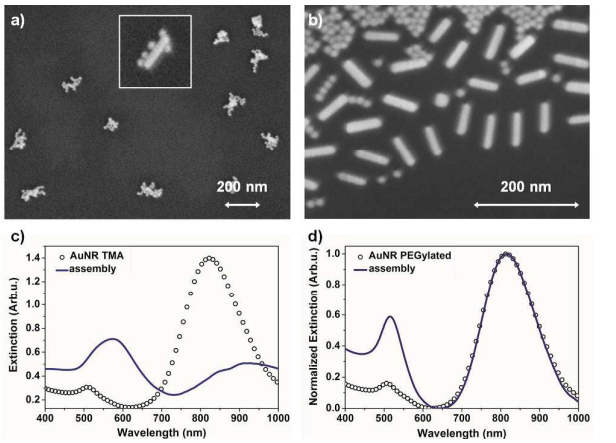

Figure 3. Representative SEM image (a) and Vis extinction spectra (c) of TMA stabilized gold after nanorod (60x16 nm) self-assembly with citrate stabilized gold nanospheres (19 nm) resulting in homogeneously coating of the nanorods (width of inset in (a): 200 nm). For fully PEGylated nanorods the spheres can not approach the nanorods based on the SEM images (b) and hence no shift in the longitudinal plasmon peaks of the nanorods could be observed in the extinction spectra (d).

View Article Online
DOI: 10.1039/C5NR08014B

At the origin of this phenomenon can be capillary forces acting upon drying, and the collapse of the PEG protecting shell when water is removed. It has to be noted, that in contrary to the SEM samples, where the rods are locked in place, in the bulk assembly experiments the nanoparticles are completely mobile, particle chain formation could cause the observed ca. 100 nm larger red-shift compared to the simulation results.[30] This difference is even larger when the bulk assembly sequence is reversed, i.e. when NP solution was pipetted into the NR solution the observed redshift increases by an additional 50 nm, which is accompanied with a significant broadening; a clear indication for pronounced chain formation in this latter case (see Supporting Information Fig S3.).

During the simulation a rod with two spherical nanoparticles located at the rod tips exactly at the long axis of the rod with a gap size of 1 nm was considered. The gap size was set as the sum of the SAM thickness for cysteamine and citrate molecules.[31,32] The two particles were moved along the rod tip perimeter to the rod side with 22.5° steps and the spectra were obtained in each position. Due to the asymmetry of the system, different light propagation and polarization directions were simulated and averaged to match closer the ensemble bulk measurement. The transversal and longitudinal modes are both affected by the angular position of the spheres. The shape of the extinction spectrum in the transversal peak region shows a marked modulation with the angular position of the spheres, resulting in a low intensity shoulder emerging around 585 nm as an indication of plasmon coupling (Figure 4.c). The longitudinal mode on the other hand redshifts by ca. 70 nm for all angular displacements. The extent of redshift is fairly independent on the angular position of the spheres, but its intensity is strongly modulated (Figure 4.d).

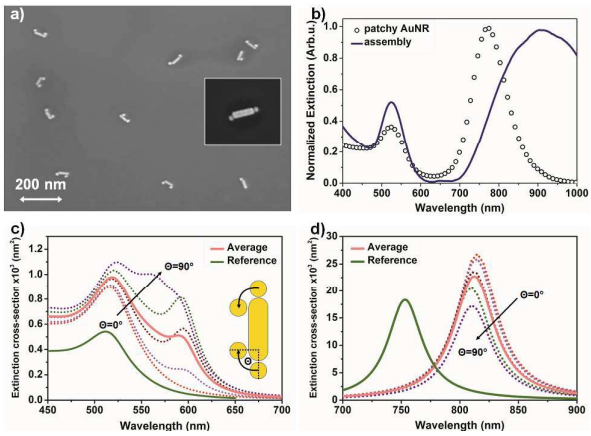

Figure 4. The SEM image of the patchy nanorods (54x15 nm) assembled with 19 nm nanospheres (a) and the corresponding extinction spectrum (b). The BEM simulations of the assembled structures with transversal (c) and longitudinal (d) excitation with respect to the nanorod long axis. The two nanospheres are moved along the tip perimeter in 22.5° steps from 0° to 90° compared to the long axis of the nanorod, maintaining a gap size of 1 nm. The dotted curves are already averaged for light propagation direction parallel and perpendicular to the plane of sphere displacement, while the solid 'Average' curve represents averaging over the different angular positions. The transversal and longitudinal extinction without nanospheres is also shown as 'Reference'.

According to the near-field images, the emerging shoulder in transversal excitation and the predicted redshift upon longitudinal excitation correspond to the evolution of coupled modes between the rod and the spheres (see Supporting Information Figure S4). Here only the results for the two spheres shifting to the same side of the rod are shown, since this matches closer the structures observed in SEM better, but when the spheres are moved to the opposite side on the rods, qualitatively the same results are obtained (see Supporting Information, Figure S5 and S6).

Although the patchy surface modification provides a robust platform to assemble small (19 nm) particles, the question arises how competing colloidal forces might influence or limit this approach? The same assembly experiment was performed with 40 nm, negatively charged (zeta potential: -30 mV) spherical particles as well. Using two additional sphere/rod size combination a markedly different behaviour was found as the particle size relative to the rod increases. First, as the sphere diameter is increased to 40 nm, the spheres are still located in the tip region of the rods with a maximum of two particles per nanorod, but the spheres are always 'bent' around the rod tip perimeter, shifted to the side (Figure 5.a). This might be interpreted again in terms of the larger van der Waals attraction associated with the side configuration, favouring this type of arrangement. For the given AuNP/AuNR sizes the difference between the tip and the side positions is around 70%, that might contribute to the evolving structure. It has to be noted, however, that drying of the sample might be also an important factor in these structural changes (i.e. bending around the NR tip). Second, as the AuNP/AuNR size ratio is further increased while keeping the rod aspect ratio the same, instead of the tip-selective localization, the particles are always positioned at the side of the rods. Additionally, only a single sphere per nanorod can be observed (Figure 5.b). For the given system the difference in the vdW attraction between the tip and the side positions is ca. 90%. An explanation for the presence of only a single sphere can be given by considering the range of electric double layer repulsion between two 40 nm diameter particles. When the two binding sites at the rod tips are further separated (Figure 5.a), the assembly of two AuNPs is allowed with a 'bent' configuration around the nanorods tip and double layer repulsion between the two spheres together with the steric repulsion provided by the PEG prevents them from side-assembly.

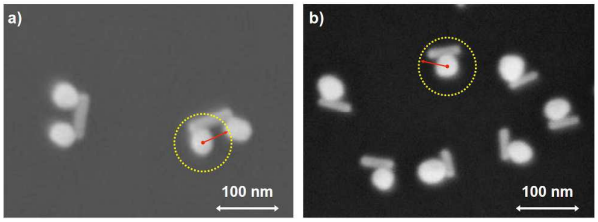

Figure 5. Assembled structures using 40 nm gold nanospheres with gold nanorods having the same aspect ratio (3.8) but different dimensions: 80x21 nm (a) and 60x16 nm (b) (also see Supporting Information Figure S7). The red arrows and the dotted circle indicate the separation distance where the value of the net particle-particle repulsion is 5 kT.

View Article Online
DOI: 10.1039/C5NR08014B

For the sample shown in Figure 5.a, the average surface-to-surface separation between the two spheres located at the same rod is 25 nm on average. This is displayed as a dotted circle around the particle (the radius of the dotted circle equals to the particle radius *plus* 25 nm surface-to-surface separation distance, i.e. 45 nm). Based on colloidal interaction calculations (Supporting Information Figure S9), bringing the second closer within the indicated zone would generate repulsion well above 5 kT. For shorter rods (Figure 5.b), however (i.e. less separated binding sites), the electric double layer repulsion seems to effectively operate over the whole extension of the rod (Figure 5.b), thus the binding of a second AuNP is not favourable. The modification of the rod tips with the positively charged molecules in this latter case is not providing a large enough driving force to overcome the repulsion of the already present particle. At the same time the absence of the second particle also allows for the more pronounced side positioning of the particle. The central role of the electric double layer interaction in the assembly process is supported by the fact that the ionic strength of the medium has a profound effect on the assembled structure. For the system shown in Figure 5.b, as salt (K_2SO_4) is added at 2.5 mM concentration (i.e. the range of the double layer repulsion between the spheres is reduced), instead of a single sphere, two particles can anchor at the same nanorod with preferential tip location (see Supporting Information Figure S8 for details). As the salt concentration further increases up to 10 mM, however, first the number of bound particle is largely reduced, and finally no spheres are assembled at the nanorods. This is consistent with the effective screening of the charges at the nanospheres and the binding sites at the rod tips. Although PEG was shown to act as an effective spacer for the small particles (Figure 3.b), from the SEM image in Figure 5.b it is clear that apparently the sphere is in close proximity of the rod. This can be a result of the distortion of the PEG layer due to the strong van der Waals interaction, but the contribution of the drying associated capillary interaction to the resulting small separation distance cannot be ruled out a priori.

For the side positioned 40 nm particle (Figure 5.b), the extinction spectrum measured during the bulk assembly process (Figure 6.a) is markedly different compared to the case where two spheres attach to a single nanorod (Figure 4.b): the longitudinal LSPR redshift is small with only a minor broadening, but the transversal mode is significantly red-shifted by 39 nm. This is consistent with the side-assembly of the spheres and the rods as observed in the SEM images. To clarify, whether the patchy nature of the rods is of importance at all for this size ratio, or is it only the van der Waals interaction that is responsible for the assembly, fully PEGylated AuNRs were used in the assembly procedure as a reference sample (Figure 6.b). In the absence of cysteamine there was no assembly taking place as the peak positions remained unchanged, hence the attractive electric double layer interaction provided by the positively charged cysteamine molecules is necessary to initiate the assembly process. BEM simulation performed for the side-assembled structure with a single sphere agrees with the results of the bulk assembly experiment, i.e. shows similar redshift and broadening of the transversal extinction (Figure 6.c) and a rather small redshift of the longitudinal mode with decreasing gap size. From the BEM calculations, the gap size in the range of 5-8 nm can be anticipated, corresponding to ca. 20 nm redshift of the transversal mode (Figure 6.c) compared to the measured 37 nm, and 15 and 26 nm shifts for the simulated and measured longitudinal modes (Figure 6.d).

Conclusions

In the present work patchy nanorods were prepared and self-assembled with nanospheres. The two step surface modification procedure resulted in two positively charged binding sites at the opposite ends of the rods, while polymer (PEG) chains were used to prevent negatively charged particle attachment in the side region of the rods. This ensured a high selectivity of the self-assembly procedure, i.e. only two spheres at the opposite tips of the rod were bound. As the sphere-to-rod size ratio increased, however, first the two bound particles were found to be significantly shifted around the perimeter of the rod's tip. For even larger sphere-to-rod size ratio, only a single sphere is attached at the side of the rods. Electrokinetic and spectroscopic data suggest that the origin of this apparent change of the assembly behaviour is a direct consequence of the inhomogeneous spatial extent and strength of colloidal interactions between the patchy rods and the spheres. The obtained results in general emphasize the need for a careful design as well as balance between patchiness, colloidal interaction strength and physical dimensions to achieve proper directionality and selectivity of pre-programmed assembly procedures.

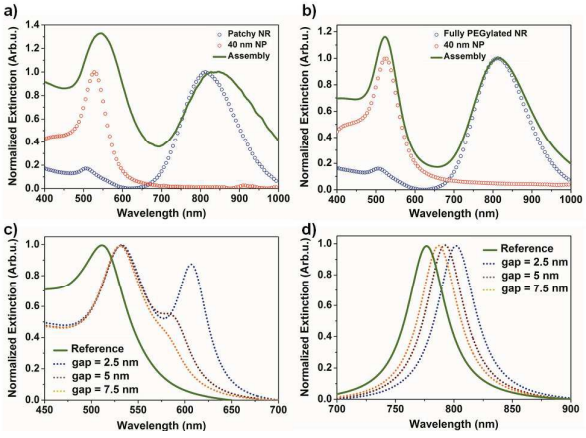

Figure 6. Experimental ensemble (a,b) and simulated (c,d) extinction spectra for the side assembled structure (see Figure 5.b): (a) bulk assembly of patchy nanorods (60x16 nm) and nanospheres (40 nm). (b) Fully PEGylated AuNR bulk assembly with nanospheres as reference experiment. Simulated spectral changes of the transversal (c) and longitudinal (d) plasmon modes assuming a single side-assembled nanosphere, with different gap sizes. The 'Reference' sample is the original plasmon peak of the nanorod.

View Article Online
DOI: 10.1039/C5NR08014B

Acknowledgements

The project was supported by the Hungarian Scientific Research Fund 'OTKA-PD-105173' and K-112114 and received funding from the European Union's Seventh Framework Programme for research, technological development and demonstration under grant agreement N° 310250. A.D. acknowledges the support of the János Bolyai Research Fellowship from the Hungarian Academy of Sciences. Sz.P. and D.Z. acknowledge the support of the Pro Progressio Foundation and József Varga Foundation.

Notes and references

1 K. J. Bishop, C. E. Wilmer, S. Soh and B. A. Grzybowski, *Small*, 2009, **5**, 1600–1630.
2 L. Xu, H. Kuang, C. Xu, W. Ma, L. Wang and N. A. Kotov, *Journal of the American Chemical Society*, 2012, **134**, 1699–1709.
3 E. Oh, M.-Y. Hong, D. Lee, S.-H. Nam, H. C. Yoon and H.-S. Kim, *Journal of the American Chemical Society*, 2005, **127**, 3270–3271.
4 A. Pearson, H. Jani, K. Kalantar-zadeh, S. K. Bhargava and V. Bansal, *Langmuir*, 2011, **27**, 6661–6667.
5 C. Wang, J. Chen, T. Talavage and J. Irudayaraj, *Angewandte Chemie International Edition*, 2009, **48**, 2759–2763.
6 K. D. Alexander, K. Skinner, S. Zhang, H. Wei and R. Lopez, *Nano Letters*, 2010, **10**, 4488–4493.
7 A. Sanchot, G. Baffou, R. Marty, A. Arbouet, R. Quidant, C. Girard and E. Dujardin, *ACS Nano*, 2012, **6**, 3434–3440.
8 Nie, D. Fava, M. Rubinstein and E. Kumacheva, *Journal of the American Chemical Society*, 2008, **130**, 3683–3689.
9 D. Baranov, L. Manna and A. G. Kanaras, *Journal of Materials Chemistry*, 2011, **21**, 16694.
10 D. Fava, Z. Nie, M. A. Winnik and E. Kumacheva, *Advanced Materials*, 2008, **20**, 4318–4322.
11 A. Lee, A. Ahmed, D. P. dos Santos, N. Coombs, J. I. Park, R. Gordon, A. G. Brolo and E. Kumacheva, *The Journal of Physical Chemistry C*, 2012, **116**, 5538–5545.
12 X. Ye, J. A. Millan, M. Engel, J. Chen, B. T. Diroll, S. C. Glotzer and C. B. Murray, *Nano Letters*, 2013, **13**, 4980–4988.
13 D. A. Walker, C. E. Wilmer, B. Kowalczyk, K. J. M. Bishop and B. A. Grzybowski, *Nano Letters*, 2010, **10**, 2275–2280.
14 D. A. Walker, E. K. Leitsch, R. J. Nap, I. Szleifer and B. A. Grzybowski, *Nature Nanotechnology*, 2013, **8**, 676–681.
15 P. Pramod, S. T. S. Joseph and K. G. Thomas, *Journal of the American Chemical Society*, 2007, **129**, 6712–6713.
16 K. Liu, A. Ahmed, S. Chung, K. Sugikawa, G. Wu, Z. Nie, R. Gordon and E. Kumacheva, *ACS Nano*, 2013, **7**, 5901–5910.
17 Z. Nie, D. Fava, E. Kumacheva, S. Zou, G. C. Walker and M. Rubinstein, *Nature Materials*, 2007, **6**, 609–614.
18 A. Lee, G. F. S. Andrade, A. Ahmed, M. L. Souza, N. Coombs, E. Tumarkin, K. Liu, R. Gordon, A. G. Brolo and E. Kumacheva, *Journal of the American Chemical Society*, 2011, **133**, 7563–7570.
19 P. Zijlstra, P. M. R. Paulo, K. Yu, Q.-H. Xu and M. Orrit, *Angewandte Chemie International Edition*, 2012, **51**, 8352–8355.
20 D. Nepal, L. F. Drummy, S. Biswas, K. Park and R. A. Vaia, *ACS Nano*, 2013, **7**, 9064–9074.
21 L. Zhong, X. Zhou, S. Bao, Y. Shi, Y. Wang, S. Hong, Y. Huang, X. Wang, Z. Xie and Q. Zhang, *Journal of Materials Chemistry*, 2011, **21**, 14448.
22 J. Turkevich, P. C. Stevenson and J. Hillier, *Discussions of the Faraday Society*, 1951, **11**, 55.
23 J. H. Yoon, J. Lim and S. Yoon, *ACS Nano*, 2012, **6**, 7199–7208.
24 W. Ni, X. Kou, Z. Yang and J. Wang, *ACS Nano*, 2008, **2**, 677–686.
25 D. Zámbó, G. Z. Radnóczi and A. Deák, *Langmuir*, 2015, **31**, 2662–2668.
26 U. Hohenester and A. Trügler, *Computer Physics Communications*, 2012, **183**, 370–381.
27 K. Liu, Z. Nie, N. Zhao, W. Li, M. Rubinstein and E. Kumacheva, *Science*, 2010, **329**, 197–200.
28 A. M. Kalsin, B. Kowalczyk, P. Wesson, M. Paszewski and B. A. Grzybowski, *Journal of the American Chemical Society*, 2007, **129**, 6664–6665.
29 X. Xia, M. Yang, Y. Wang, Y. Zheng, Q. Li, J. Chen and Y. Xia, *ACS Nano*, 2012, **6**, 512–522.
30 A. Lukach, K. Liu, H. Therien-Aubin and E. Kumacheva, *Journal of the American Chemical Society*, 2012, **134**, 18853–18859.
31 P. Mulvaney, L. M. Liz-Marzán, M. Giersig and T. Ung, *Journal of Materials Chemistry*, 2000, **10**, 1259–1270.
32 P. Tengvall, M. Lestelius, B. Liedberg and I. Lundstroem, *Langmuir*, 1992, **8**, 1236–1238.